

## Observation of nearly identical superconducting transition temperatures in the pressurized Weyl semimetals $M\text{IrTe}_4$ ( $M = \text{Nb}$ and $\text{Ta}$ )

Sijin Long,<sup>1,2,\*</sup> Shu Cai,<sup>1,\*</sup> Rico Schönemann<sup>3</sup>, Priscila F. S. Rosa,<sup>3</sup> Luis Balicas,<sup>4</sup> Cheng Huang<sup>5</sup>,<sup>1,2</sup> Jing Guo,<sup>1,5</sup> Yazhou Zhou,<sup>1</sup> Jinyu Han,<sup>1,2</sup> Liqin Zhou,<sup>1,2</sup> Yanchun Li,<sup>6</sup> Xiaodong Li,<sup>6</sup> Qi Wu,<sup>1</sup> Hongming Weng,<sup>1,2</sup> Tao Xiang,<sup>1,2,5</sup> and Liling Sun<sup>1,2,5,†</sup>

<sup>1</sup>*Institute of Physics, National Laboratory for Condensed Matter Physics, Chinese Academy of Sciences, Beijing 100190, China*

<sup>2</sup>*Department of Physics, University of Chinese Academy of Sciences, Beijing 100190, China*

<sup>3</sup>*MPA-MAGLAB, Los Alamos National Laboratory, Los Alamos, New Mexico 87545, USA*

<sup>4</sup>*National High Magnetic Field Laboratory, Tallahassee, Florida 32310, USA*

<sup>5</sup>*Songshan Lake Materials Laboratory, Dongguan, Guangdong 523808, China*

<sup>6</sup>*Institute of High Energy Physics, Chinese Academy of Science, Beijing 100049, China*



(Received 20 April 2021; revised 26 August 2021; accepted 28 September 2021; published 11 October 2021)

Here, we report the observation of pressure-induced superconductivity in type-II Weyl semimetal (WSM) candidate  $\text{NbIrTe}_4$  and the evolution of its Hall coefficient ( $R_H$ ), magnetoresistance (MR), and lattice with increasing pressure to  $\sim 63$  GPa. These results provide a significant opportunity to investigate the universal high-pressure (HP) behavior of ternary WSMs, including the sister compound  $\text{TaIrTe}_4$  that has been known through our previous studies. We find that the pressure-tuned evolution from the WSM to the superconducting (SC) state in these two compounds exhibits the same trend, i.e., a pressure-induced SC state emerges from the matrix of the non-SC WSM state at  $\sim 27$  GPa, and then the WSM and SC states coexist up to 40 GPa. Above this pressure, an identical HP behavior, characterized by almost the same value of  $R_H$  and MR in its normal state and the same value of  $T_c$  in its SC state, appears in both compounds. Our results not only reveal the evolution from the WSM state to the SC state but also demonstrate that  $\text{NbIrTe}_4$  and  $\text{TaIrTe}_4$  can make the same contribution to the normal and SC states that inhabit the HP phase, although these two compounds have dramatically different band structure at ambient pressure.

DOI: [10.1103/PhysRevB.104.144503](https://doi.org/10.1103/PhysRevB.104.144503)

Weyl semimetals (WSMs) have recently attracted extensive attention in the field of condensed matter physics and material science since Weyl fermions have not been observed so far as a fundamental particle in high energy physics [1–5]. In condensed matter physics, the WSM is accepted as a topologically nontrivial metallic phase, where Weyl fermions emerge as quasiparticles from linear crossing bands [1,6,7]. Two types of WSMs have been predicted theoretically [1,8–11] and identified experimentally [3,12,13]. The materials of  $MX$  ( $M = \text{Ta}, \text{Nb}$  and  $X = \text{As}, \text{P}$ ) are classified as type-I WSMs, characterized by a pointlike Fermi surface at the Weyl node. While type-II WSMs can be found in the transition-metal dichalcogenide family, which includes the compounds of  $M\text{Te}_2$  as well as  $MP_2$  ( $M = \text{W}, \text{Mo}$ ) and the ternary variants of  $MX\text{Te}_4$  ( $M = \text{Ta}, \text{Nb}$  and  $X = \text{Ir}, R_h$ ) [5,11,14–16]. The electronic structure of the WSMs gives rise to fascinating phenomena in transport properties, such as a chiral anomaly in the presence of parallel electric and magnetic fields leading to negative magnetoresistance (MR), anomalous Hall response, surface-state quantum oscillations, and exotic superconductivity [17–24]. These properties of the

WSMs establish them as a platform for exploring potential applications in nonlinear optics.

Like the lattice structure of  $\text{TaIrTe}_4$ ,  $\text{NbIrTe}_4$  also crystallizes in an orthorhombic (OR) unit cell with the  $Pmn2_1$  space group and can be viewed as a cell-doubling derivative [5,15]. Theoretical calculations indicate that  $\text{NbIrTe}_4$  has a more complicated electronic structure (16 Weyl points in the Brillouin zone) [5] than  $\text{TaIrTe}_4$  (4 Weyl points in the Brillouin zone) [15,25]. The presence of Weyl points in  $\text{NbIrTe}_4$ , accompanied by the common features of a large nonsaturating MR effect, have been supported experimentally [26]. Pressure is an important tuning parameter that can be utilized to alter the lattice and corresponding electronic structures of a material and therefore influence its electrical transport properties. It is our goal to gain a deeper insight into the nature of WSMs and to achieve a better understanding of the connection between its nontrivial WSM and superconducting (SC) states. Compelling examples of pressure-induced SC transition have been observed in the type-II WSM  $\text{WTe}_2$  [27,28],  $T_d$ - $\text{MoTe}_2$ , and  $\text{MoTe}_{2-x}\text{S}_x$  [20,29,30]. As a ternary variant of  $\text{WTe}_2$ ,  $\text{TaIrTe}_4$  has also displayed superconductivity at high pressures [31] and surface superconductivity [32]. The high-pressure (HP) behavior of the WSM  $\text{NbIrTe}_4$  remains unknown, and the connection between the WSM and SC states in the ternary WSMs as a function of lattice changes is an open question. In this paper, we reveal the evolution of pressure-induced

\*These authors contributed equally to this work.

†Corresponding author: [llsun@iphy.ac.cn](mailto:llsun@iphy.ac.cn)

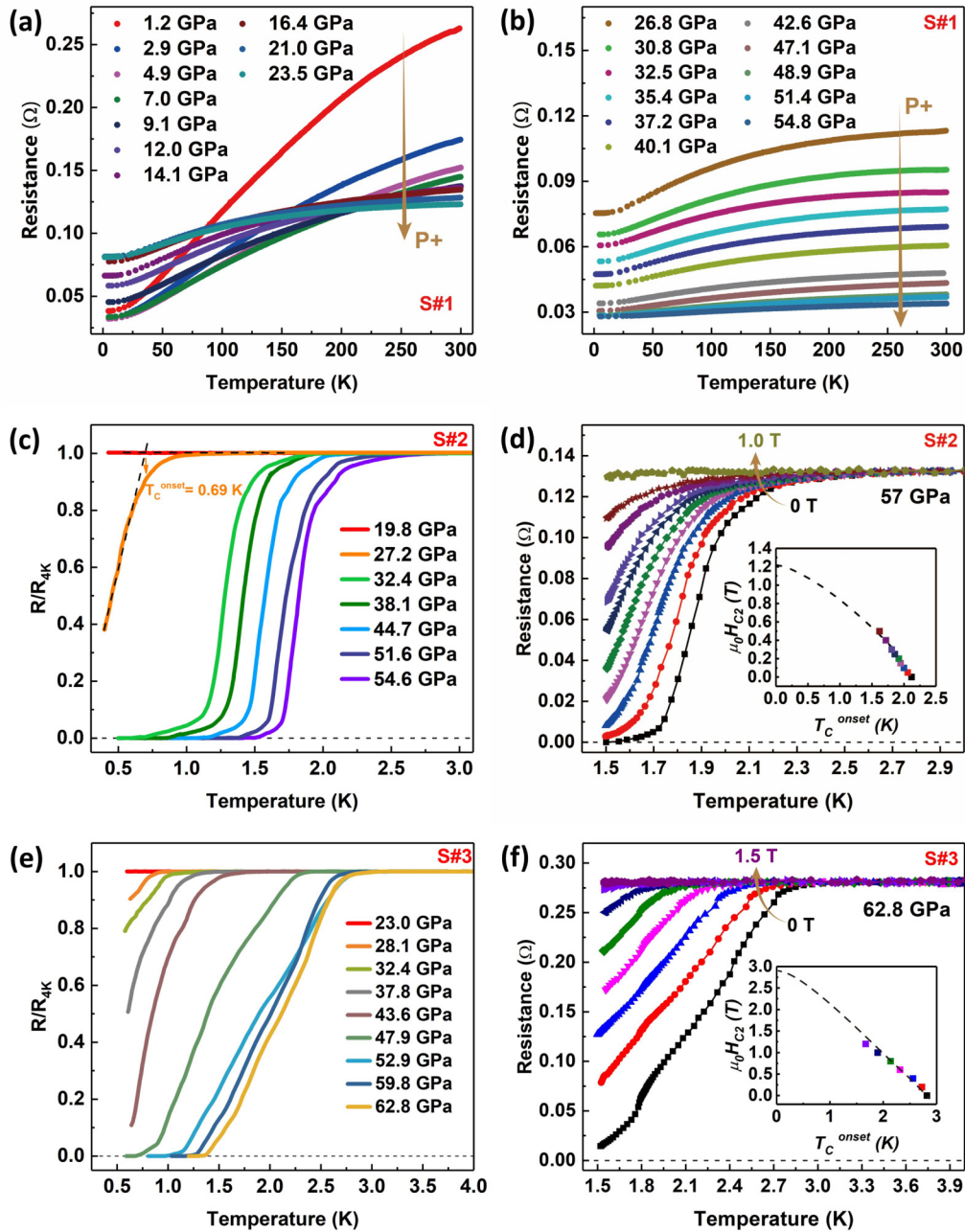


FIG. 1. Temperature dependence of electrical resistance at different pressures and magnetic fields. (a) and (b) The resistance as a function of temperature for sample 1 (S#1) measured over the range of 1.5–300 K at different pressures. (c) and (e) The resistance vs temperature for sample 2 (S#2) and sample 3 (S#3) measured in the range of 0.35–4 K at different pressures, showing the superconducting (SC) transition. (d) and (f) Magnetic field dependence of the SC transition temperature measured at 57 and 62.8 GPa for S#2 and S#3, respectively. The insets of (d) and (f) show the dependence of upper critical field.

superconductivity from the ambient pressure WSM state in  $\text{NbIrTe}_4$  and compare our results with those observed in  $\text{TaIrTe}_4$ .

High-quality single crystals of  $\text{NbIrTe}_4$  were grown by a Te flux method as described in Ref. [26]. The scanning electron microscope (SEM) mapping and energy dispersive spectrometer (EDS) analysis on the  $\text{NbIrTe}_4$  single crystal were carried out before HP experiments. The results of the SEM mapping show that the constituent elements (Nb, Ir, and Te) distribute homogeneously in the single crystal (see the Supplemental Material [33]). The EDS analysis shows

that the stoichiometry of the sample used in this paper is  $\text{Nb}_{1.1}\text{Ir}_{0.96}\text{Te}_{4.04}$  (see the Supplemental Material [33]), very close to the 1:1:4 stoichiometry. Figures 1(a) and 1(b) show the temperature ( $T$ ) dependence of the electrical resistance ( $R$ ) measured in a  $\text{NbIrTe}_4$  sample (S#1) under pressures to 54.8 GPa within the temperature range of 1.5–300 K. Over the pressure range investigated,  $R(T)$  displays metallic behavior, as observed at ambient pressure. The details of the HP measurements on S#1 can be found in the Supplemental Material [33]. The pressure for measurements was determined by the ruby fluorescence method [34] and the shift of

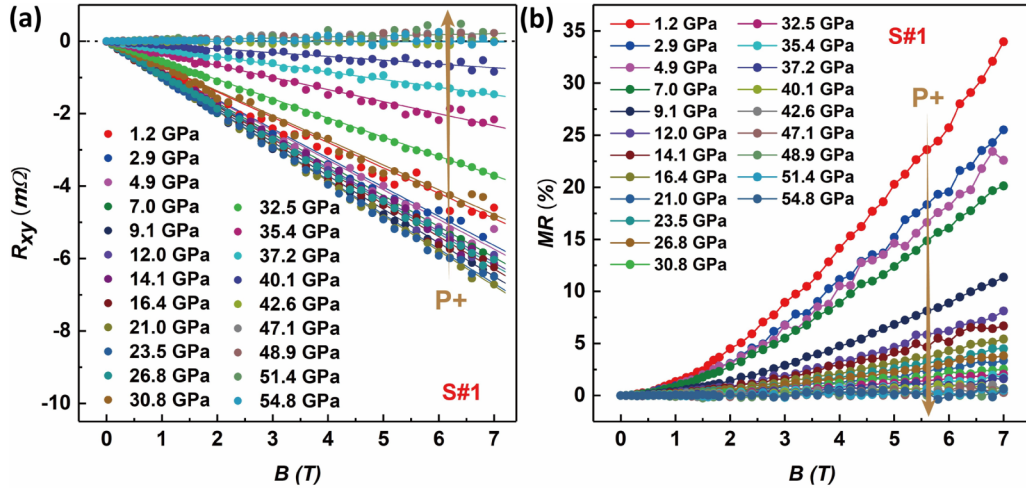


FIG. 2. Results of Hall and magnetoresistance (MR) obtained from NbIrTe<sub>4</sub>. (a) Hall resistance ( $R_{xy}$ ) as a function of magnetic field at different pressures, displaying that  $R_{xy}(B)$  exhibits a slow change <26.8 GPa, then increases above this pressure and tends to zero upon further compression. (b) Magnetic field dependence of MR [MR(%)] for pressures ranging from 1.2 to 54.8 GPa {here MR(%) =  $[R(7T) - R(0T)]/R(0T) \times 100\%$ }, showing that MR(%) decreases with increasing pressure.

diamond Raman [35,36]. Considering the anisotropic transport property of the  $M\text{IrTe}_4$  ( $M = \text{Ta}$  and  $\text{Nb}$ ), i.e., the resistance along the  $b$  axis ( $R_b$ ) is much higher than that along the  $a$  axis ( $R_a$ ) [37], in the studies on sample 2 (S#2), we not only ascertained the crystal orientation before loading the sample into the HP cell but also adopted the standard four-electrode method for getting reliable data (see the geometry of the standard four-probe method in the Supplemental Material [33]). The resistance measurements on S#2 were performed in a <sup>3</sup>He cryostat down to 0.35 K. A resistance drop with the transition temperature of  $\sim 0.69$  K was found at 27.2 GPa [Fig. 1(c)]. Upon further compression, a zero-resistance state was observed at pressures  $\sim 32.4$  GPa [Fig. 1(c)], indicating a SC transition. The transition temperature increased with pressure and reached 1.94 K at 54.6 GPa. To further characterize whether the pressure-induced resistance drop is associated with a SC transition, we applied a magnetic field along the interplanar direction at 57 GPa. As shown in Fig. 1(d), the transition shifts to lower temperatures upon increasing the magnetic field, indicating that the observed resistance drop indeed originates from a SC transition. We estimated the upper critical magnetic field ( $H_{c2}$ ) for the SC phase of NbIrTe<sub>4</sub> by using the Werthamer-Helfand-Hohenberg (WHH) formula [38]:  $H_{c2}^{\text{WHH}}(0) = -0.693 T_c (dH_{c2}/dT)_{T=T_c}$ , which yields an upper critical field of  $\sim 1.2$  T at 57 GPa [inset of Fig. 1(d)]. We repeated the measurements on another sample (S#3) in the same experimental manner as that of S#2 and found that the pressure-induced SC transition in NbIrTe<sub>4</sub> is reproducible (Figs. 1(e) and 1(f), as well as the Supplemental Material [33]). The SC transition starting at 28.1 GPa was observed, and the superconductivity prevailed in the pressure range up to 62.8 GPa. The upper critical magnetic field ( $H_{c2}$ ) for the SC phase at 62.8 GPa was  $\sim 3$  T [see inset of Fig. 1(f)], slightly higher than that obtained at 57 GPa [Fig. 1(d)].

To understand the connection between the superconductivity and the WSM state in NbIrTe<sub>4</sub>, we performed HP measurements of the Hall resistance ( $R_{xy}$ ) by sweeping the magnetic field ( $B$ ), which is applied perpendicular to the  $ab$

plane, from 0 to 7 T at 10 K. As shown in Fig. 2(a),  $R_{xy}(B)$  is negative within the pressure range investigated, indicating that electrons are the dominant charge carriers at the Fermi surface. Upon increasing pressure, the slope of  $R_{xy}(B)$  becomes smaller and approaches zero at pressures  $>40$  GPa. These results suggest that the shrinkage of the lattice by applying pressure likely adjusts the carrier density in these two materials, leading to  $R_{xy}(B) = 0$  eventually.

The emergence of superconductivity in WSMs is closely associated with a suppression of MR [27,28,31]. To reveal the connection between superconductivity and positive MR effect in NbIrTe<sub>4</sub>, we carried out MR measurements on our sample at 10 K in the pressure range of 1.2–54.8 GPa. As shown in Fig. 2(b), the ambient pressure NbIrTe<sub>4</sub> shows a positive MR {MR(%) = 35% at 1.2 GPa; here, MR(%) is determined by  $[R(7T) - R(0T)]/R(0T) \times 100\%$ }, which can be suppressed dramatically by pressure. In the presence of superconductivity at  $\sim 27$  GPa, the value of MR(%) is  $\sim 3.3\%$ .

The transport property of materials is usually influenced by the type of crystal structure. To understand why the value of MR does not reach zero at the critical pressure of SC transition, we performed HP x-ray diffraction measurements. As shown in Fig. 3, all diffraction peaks gradually shift to higher angles upon increasing pressure, and the patterns can be indexed well with the OR structure ( $Pmn2_1$  space group)  $<24.8$  GPa. At 27.5 GPa, there are two new peaks present [Fig. 3(b), as indicated by stars]. Although the intensity of these new peaks becomes more pronounced with elevating pressure, we are unable to determine the structure for this new phase through only two peaks. As a result, we define the new phase as the HP phase in this paper. These results show that the HP phase which emerged from the matrix of the ambient pressure (OR) phase and coexisted with the OR phase in the pressure range of 27.5–40.4 GPa is responsible for the nonzero MR state and the presence of the SC state. When pressure is increased  $>40.4$  GPa, we cannot index the peaks by the OR phase, implying that the OR phase completely transforms to the HP phase at this pressure, where MR reaches

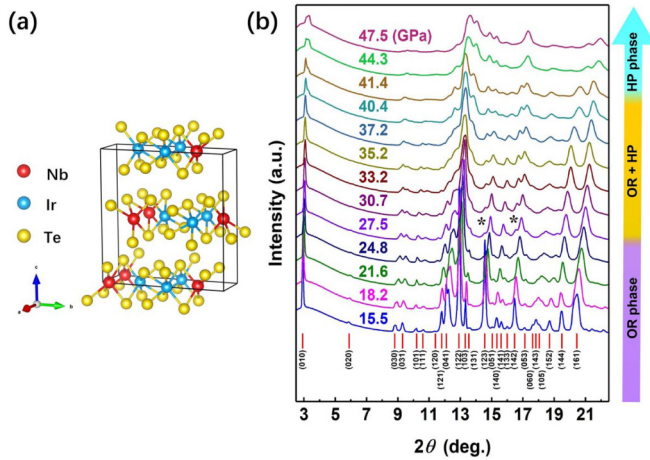


FIG. 3. (a) Schematic crystal structure of NbIrTe<sub>4</sub>. (b) X-ray diffraction patterns collected at different pressures. In the range of 15–27 GPa, the sample remains orthorhombic (OR) phase (see violet regime), while in the range of 27.5–40.4 GPa, it hosts a mixed phase composed of OR and high-pressure (HP) phases (see the orange regime). Upon further compression, the sample possesses a pure HP phase (see the cyan regime).

zero. In the sister compound TaIrTe<sub>4</sub>, the pressure-induced SC state is also accompanied by a lattice distortion [31]. These results suggest that the structural change from the OR phase to the HP phase is responsible for development of the superconductivity in NbIrTe<sub>4</sub>. When pressure is >40 GPa, the OR phase that protects the WSM state converts to the HP phase completely; thus, the WSM state no longer exists (Fig. 3). Our results suggest that the topology of the WSM is likely not beneficial for developing the superconductivity in the pressurized NbIrTe<sub>4</sub> and TaIrTe<sub>4</sub>.

We summarize our HP experimental results in Fig. 4. It is found that three distinct regimes can be seen in the  $P$ - $T$  diagram: the WSM state (on the left), the mixed state of the WSM and SC states (in the middle), and the SC state (on the right). In the left regime [below the critical pressure ( $P_{c1}$ )], NbIrTe<sub>4</sub> remains in the OR structure (Fig. 3), and its ground state is a WSM. Within this pressure range,  $R_H$  displays a

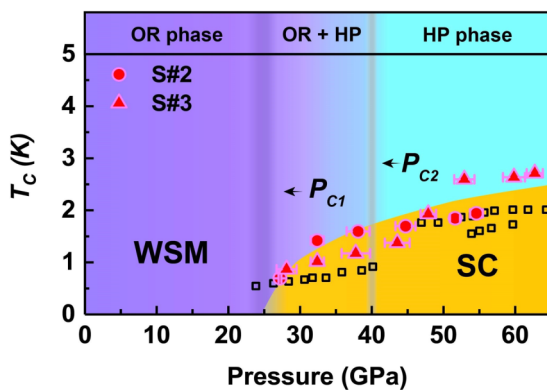


FIG. 4. Pressure –  $T_c$  phase diagram with structure information for NbIrTe<sub>4</sub>. The data of TaIrTe<sub>4</sub> (see black squares taken from Ref. [31]) is included for comparison. WSM and SC represent Weyl semimetal and superconducting states, respectively.

slow variation (see the Supplemental Material [33]), but MR shows a monotonic decrease with increasing pressure (see the Supplemental Material [33]). At  $P_{c1}$ , a HP phase emerges from the matrix of the OR phase, accompanied by the presence of superconductivity. Concomitantly, the value of  $R_H$  starts to approach zero, and MR(%) decreases to 3.3% (see the Supplemental Material [33]). In the middle regime (27–40 GPa), a mixed state composed of the WSM state, characterized by the OR phase (Fig. 3) as well as positive MR [Fig. 2(b)], and the SC state is observed. In the HP regime (40–57 GPa), MR(%) of NbIrTe<sub>4</sub> reaches zero, and the OR-to-HP phase transition finishes [Figs. 2(b) and 3], implying that the ground state becomes a pure SC state.

To visualize the HP behavior of these two materials, we compare the data obtained from NbIrTe<sub>4</sub> and TaIrTe<sub>4</sub> (see black squares taken from Ref. [31]) in Fig. 4. The critical pressure ( $P_{c1}$ ) of the SC transition for NbIrTe<sub>4</sub> and TaIrTe<sub>4</sub> is almost the same. Although the sign of their ambient pressure  $R_H$  is different, both  $R_H$  change their trend when superconductivity appears (see the Supplemental Material [33]). Moreover, at the critical pressure ( $P_{c2}$ ) and above, not only MR(%) of the two materials reaches zero, but also their  $R_H$  and  $T_c$  surprisingly merge into almost the same values (see the Supplemental Material [33]). These results suggest that, although NbIrTe<sub>4</sub> and TaIrTe<sub>4</sub> possess dramatically different band structures at ambient pressure, the very similar HP behaviors of these two materials may be attributed to pressure assimilating their crystal and electronic structure. Our results support the previous theoretical calculations on  $M$ IrTe<sub>4</sub> ( $M = \text{Ta}$  and  $\text{Nb}$ ) that their topological band structure can be remarkably modified by the volume shrinkage [25,39]. Because Nb and Ta have very similar ion radius but quite different mass ( $m_{\text{Nb}} = 93$ , while  $m_{\text{Ta}} = 181$ ), these features may empower them as a unique platform to “simulate isotope effect,” i.e., the effect of mass change on the phonon and corresponding  $T_c$ , for understanding the SC mechanism. Subsequently, a fundamental question is raised: What is the key factor for determining the SC and normal states in these pressurized WSMs? Also, can the superconductivity found in  $M$ IrTe<sub>4</sub> ( $M = \text{Nb}$  and  $\text{Ta}$ ) fall into the unconventional superconductivity category? Moreover, it is noteworthy to ask the question about what the transport properties and the electronic state look like at the boundary of the WSM and SC states when they coexist. All call for further investigators from theoretical and experimental sides.

In summary, we report the observation of superconductivity in pressurized type-II WSM candidate NbIrTe<sub>4</sub>, through the complementary measurements of HP resistance, Hall coefficient, MR, and synchrotron X-ray diffraction. The pressure-induced superconductivity state with the transition temperature ( $T_c$ ) of  $\sim 0.69$  K emerges from the matrix of the WSM state at 27.2 GPa. The WSM and SC states coexist in the pressure range of 27–40 GPa. Then a pure SC state remains in the range of 40–62.8 GPa. By comparing NbIrTe<sub>4</sub> and TaIrTe<sub>4</sub>, we find a remarkably similar evolution process, from a WSM-OR phase to a SC-HP phase, in these two compounds. Intriguingly, the values of  $R_H$ , MR(%), and  $T_c$  of NbIrTe<sub>4</sub> and TaIrTe<sub>4</sub> seem the same at  $\sim 40$  GPa and above. Our HP results not only reveal the universal connection among the lattice structure, superconductivity, and the band structure in these

two WSMs but also demonstrate that pressure can tune these two WSMs to have nearly the identical normal and SC properties. Such an unconventional behavior of superconductivity, independence of the mass of Nb and Ta ions is of great interest and deserves investigations in the future.

*Note added.* Recently, a related work was brought to our attention [40].

The work in China was supported by the National Natural Science Foundation (NSF) of China (Grants No. U2032214, No. 11888101, and No. 12004419), the Strategic Priority Research Program (B) of the Chinese Academy of Sciences (Grant No. XDB25000000), and the National Key Research and Development Program of China (Grants No. 2017YFA0302900 and No. 2017YFA0303103). We are

thankful for the support from the Users with Excellence Program of Hefei Science Center CAS (No. 2020HSC-UE015). Part of the work is supported by the Synergic Extreme Condition User System. S.C. and J. G. are grateful for support from the China Postdoctoral Science Foundation (No. E0BK111) and the Youth Innovation Promotion Association of the CAS (No. 2019008). L.B. is supported by the U.S. Department of Energy (DOE), Basic Energy Sciences (BES) through Award No. DE-SC0002613. The work at Los Alamos National Laboratory was supported by the Center for Integrated Nanotechnologies, and Office of Science User Facility operated for the DOE, Office of Science. A portion of this work was performed at the National High Magnetic Field Laboratory, which is supported by the NSF Cooperative Agreement No. DMR-1644779, the DOE, and the State of Florida.

- 
- [1] X. Wan, A. M. Turner, A. Vishwanath, and S. Y. Savrasov, Topological semimetal and Fermi-arc surface states in the electronic structure of pyrochlore iridates, *Phys. Rev. B* **83**, 205101 (2011).
- [2] A. A. Burkov and L. Balents, Weyl Semimetal in a Topological Insulator Multilayer, *Phys. Rev. Lett.* **107**, 127205 (2011).
- [3] S.-Y. Xu, I. Belopolski, N. Alidoust, M. Neupane, G. Bian, C. Zhang, R. Sankar, G. Chang, Z. Yuan, C.-C. Lee, S.-M. Huang, H. Zheng, J. Ma, D. S. Sanchez, B. Wang, A. Bansil, F. Chou, P. P. Shibayev, H. Lin, S. Jia *et al.*, Discovery of a Weyl fermion semimetal and topological Fermi arcs, *Science* **9**, 613 (2015).
- [4] L. Lu, Z. Wang, D. Ye, L. Ran, L. Fu, J. D. Joannopoulos, and M. Soljačić, Experimental observation of Weyl points, *Science* **9**, 622 (2015).
- [5] L. Li, H.-H. Xie, J.-S. Zhao, X.-X. Liu, J.-B. Deng, X.-R. Hu, and X.-M. Tao, Ternary Weyl semimetal NbIrTe<sub>4</sub> proposed from first-principles calculation, *Phys. Rev. B* **96**, 024106 (2017).
- [6] M. Z. Hasan and C. L. Kane, Colloquium: Topological insulators, *Rev. Mod. Phys.* **82**, 3045 (2010).
- [7] X.-L. Qi and S.-C. Zhang, Topological insulators and superconductors, *Rev. Mod. Phys.* **83**, 1057 (2011).
- [8] H. Weng, C. Fang, Z. Fang, B. A. Bernevig, and X. Dai, Weyl Semimetal Phase in Noncentrosymmetric Transition-Metal Monophosphides, *Phys. Rev. X* **5**, 011029 (2015).
- [9] G. Xu, H. Weng, Z. Wang, X. Dai, and Z. Fang, Chern Semimetal and the Quantized Anomalous Hall Effect in HgCr<sub>2</sub>Se<sub>4</sub>, *Phys. Rev. Lett.* **107**, 186806 (2011).
- [10] S.-M. Huang, S.-Y. Xu, I. Belopolski, C.-C. Lee, G. Chang, B. Wang, N. Alidoust, G. Bian, M. Neupane, C. Zhang, S. Jia, A. Bansil, H. Lin, and M. Z. Hasan, A Weyl fermion semimetal with surface Fermi arcs in the transition metal monophosphides TaAs class, *Nat. Commun.* **6**, 7373 (2015).
- [11] A. A. Soluyanov, D. Gresch, Z. Wang, Q. Wu, M. Troyer, X. Dai, and B. A. Bernevig, Type-II Weyl semimetals, *Nature (London)* **527**, 495 (2015).
- [12] L. X. Yang, Z. K. Liu, Y. Sun, H. Peng, H. F. Yang, T. Zhang, B. Zhou, Y. Zhang, Y. F. Guo, M. Rahn, D. Prabhakaran, Z. Hussain, S. K. Mo, C. Felser, B. Yan, and Y. L. Chen, Weyl semimetal phase in the non-centrosymmetric compound TaAs, *Nat. Phys.* **11**, 728 (2015).
- [13] B. Q. Lv, H. M. Weng, B. B. Fu, X. P. Wang, H. Miao, J. Ma, P. Richard, X. C. Huang, L. X. Zhao, G. F. Chen, Z. Fang, X. Dai, T. Qian, and H. Ding, Experimental Discovery of Weyl Semimetal TaAs, *Phys. Rev. X* **5**, 031013 (2015).
- [14] Y. Sun, S.-C. Wu, M. N. Ali, C. Felser, and B. Yan, Prediction of Weyl semimetal in orthorhombic MoTe<sub>2</sub>, *Phys. Rev. B* **92**, 161107(R) (2015).
- [15] K. Koepf, D. Kasinathan, D. V. Efremov, S. Khim, S. Borisenko, B. Büchner, and J. van den Brink, TaIrTe<sub>4</sub>: A ternary type-II Weyl semimetal, *Phys. Rev. B* **93**, 201101(R) (2016).
- [16] G. Autès, D. Gresch, M. Troyer, A. A. Soluyanov, and O. V. Yazyev, Robust Type-II Weyl Semimetal Phase in Transition Metal Diphosphides X<sub>2</sub>P<sub>2</sub> (X = Mo, W), *Phys. Rev. Lett.* **117**, 066402 (2016).
- [17] X. Huang, L. Zhao, Y. Long, P. Wang, D. Chen, Z. Yang, H. Liang, M. Xue, H. Weng, Z. Fang, X. Dai, and G. Chen, Observation of the Chiral-Anomaly-Induced Negative Magnetoresistance in 3D Weyl Semimetal TaAs, *Phys. Rev. X* **5**, 031023 (2015).
- [18] A. A. Zyuzin and A. A. Burkov, Topological response in Weyl semimetals and the chiral anomaly, *Phys. Rev. B* **86**, 115133 (2012).
- [19] A. C. Potter, I. Kimchi, and A. Vishwanath, Quantum oscillations from surface Fermi arcs in Weyl and Dirac semimetals, *Nat. Commun.* **5**, 5161 (2014).
- [20] Y. Qi, P. G. Naumov, M. N. Ali, C. R. Rajamathi, W. Schnelle, O. Barkalov, M. Hanfland, S.-C. Wu, C. Shekhar, Y. Sun, V. Süß, M. Schmidt, U. Schwarz, E. Pippel, P. Werner, R. Hillebrand, T. Förster, E. Kampert, S. Parkin, R. J. Cava *et al.*, Superconductivity in Weyl semimetal candidate MoTe<sub>2</sub>, *Nat. Commun.* **7**, 11038 (2016).
- [21] F. C. Chen, X. Luo, R. C. Xiao, W. J. Lu, B. Zhang, H. X. Yang, J. Q. Li, Q. L. Pei, D. F. Shao, R. R. Zhang, L. S. Ling, C. Y. Xi, W. H. Song, and Y. P. Sun, Superconductivity enhancement in the S-doped Weyl semimetal candidate MoTe<sub>2</sub>, *Appl. Phys. Lett.* **108**, 162601 (2016).
- [22] L. Zhu, Q.-Y. Li, Y.-Y. Lv, S. Li, X.-Y. Zhu, Z.-Y. Jia, Y. B. Chen, J. Wen, and S.-C. Li, Superconductivity in Potassium-Intercalated T<sub>d</sub>-WTe<sub>2</sub>, *Nano Lett.* **18**, 6585 (2018).

- [23] V. Fatemi, S. Wu, Y. Cao, L. Bretheau, Q. D. Gibson, K. Watanabe, T. Taniguchi, R. J. Cava, and P. Jarillo-Herrero, Electrically tunable low-density superconductivity in a monolayer topological insulator, *Science* **362**, 926 (2018).
- [24] E. Sajadi, T. Palomaki, Z. Fei, W. Zhao, P. Bement, C. Olsen, S. Luescher, X. Xu, J. A. Folk, and D. H. Cobden, Gate-induced superconductivity in a monolayer topological insulator, *Science* **362**, 922 (2018).
- [25] X. Zhou, Q. Liu, Q. Wu, T. Nummy, H. Li, J. Griffith, S. Parham, J. Waugh, E. Emmanouilidou, B. Shen, O. V. Yazyev, N. Ni, and D. Dessau, Coexistence of tunable Weyl points and topological nodal lines in ternary transition-metal telluride TaIrTe<sub>4</sub>, *Phys. Rev. B* **97**, 241102(R) (2018).
- [26] R. Schönemann, Y.-C. Chiu, W. Zheng, V. L. Quito, S. Sur, G. T. McCandless, J. Y. Chan, and L. Balicas, Bulk Fermi surface of the Weyl type-II semimetallic candidate NbIrTe<sub>4</sub>, *Phys. Rev. B* **99**, 195128 (2019).
- [27] D. Kang, Y. Zhou, W. Yi, C. Yang, J. Guo, Y. Shi, S. Zhang, Z. Wang, C. Zhang, S. Jiang, A. Li, K. Yang, Q. Wu, G. Zhang, L. Sun, and Z. Zhao, Superconductivity emerging from a suppressed large magnetoresistant state in tungsten ditelluride, *Nat. Commun.* **6**, 7804 (2015).
- [28] X.-C. Pan, X. Chen, H. Liu, Y. Feng, Z. Wei, Y. Zhou, Z. Chi, L. Pi, F. Yen, F. Song, X. Wan, Z. Yang, B. Wang, G. Wang, and Y. Zhang, Pressure-driven dome-shaped superconductivity and electronic structural evolution in tungsten ditelluride, *Nat. Commun.* **6**, 7805 (2015).
- [29] Z. Guguchia, F. von Rohr, Z. Shermadini, A. T. Lee, S. Banerjee, A. R. Wieteska, C. A. Marianetti, B. A. Frandsen, H. Luetkens, Z. Gong, S. C. Cheung, C. Baines, A. Shengelaya, G. Taniashvili, A. N. Pasupathy, E. Morenzoni, S. J. L. Billinge, A. Amato, R. J. Cava, R. Khasanov *et al.*, Signatures of the topological  $s+-$  superconducting order parameter in the type-II Weyl semimetal T<sub>d</sub>-MoTe<sub>2</sub>, *Nat. Commun.* **8**, 1082 (2017).
- [30] Y. Li, Q. Gu, C. Chen, J. Zhang, Q. Liu, X. Hu, J. Liu, Y. Liu, L. Ling, M. Tian, Y. Wang, N. Samarth, S. Li, T. Zhang, J. Feng, and J. Wang, Nontrivial superconductivity in topological MoTe<sub>2-x</sub>S<sub>x</sub> crystals, *Proc. Natl. Acad. Sci.* **115**, 9503 (2018).
- [31] S. Cai, E. Emmanouilidou, J. Guo, X. Li, Y. Li, K. Yang, A. Li, Q. Wu, N. Ni, and L. Sun, Observation of superconductivity in the pressurized Weyl-semimetal candidate TaIrTe<sub>4</sub>, *Phys. Rev. B* **99**, 020503(R) (2019).
- [32] Y. Xing, Z. Shao, J. Ge, J. Luo, J. Wang, Z. Zhu, J. Liu, Y. Wang, Z. Zhao, J. Yan, D. Mandrus, B. Yan, X.-J. Liu, M. Pan, and J. Wang, Surface superconductivity in the type II Weyl semimetal TaIrTe<sub>4</sub>, *Natl. Sci. Rev.* **7**, 579 (2020).
- [33] See Supplemental Material at <http://link.aps.org/supplemental/10.1103/PhysRevB.104.144503> for the HP experimental details and extended results.
- [34] H. K. Mao, J. Xu, and P. M. Bell, Calibration of the ruby pressure gauge to 800 kbar under quasi-hydrostatic conditions, *J. Geophys. Res.: Solid Earth* **91**, 4673 (1986).
- [35] L. Sun, A. L. Ruoff, and G. Stupian, Convenient optical pressure gauge for multimegabar pressures calibrated to 300 GPa, *Appl. Phys. Lett.* **86**, 014103 (2004).
- [36] Y. Akahama and H. Kawamura, Pressure calibration of diamond anvil Raman gauge to 310 GPa, *J. Appl. Phys.* **100**, 043516 (2006).
- [37] Y. Liu, Q. Gu, Y. Peng, S. Qi, N. Zhang, Y. Zhang, X. Ma, R. Zhu, L. Tong, J. Feng, Z. Liu, and J.-H. Chen, Raman signatures of broken inversion symmetry and in-plane anisotropy in type-II Weyl semimetal candidate TaIrTe<sub>4</sub>, *Adv. Mater.* **30**, 1706402 (2018).
- [38] N. R. Werthamer, E. Helfand, and P. C. Hohenberg, Temperature and purity dependence of the superconducting critical field,  $H_{c2}$ . III. Electron spin and spin-orbit effects, *Phys. Rev.* **147**, 295 (1966).
- [39] J. Liu, H. Wang, C. Fang, L. Fu, and X. Qian, van der Waals stacking-induced topological phase transition in layered ternary transition metal chalcogenides, *Nano Lett.* **17**, 467 (2017).
- [40] Q.-G. Mu, F.-R. Fan, H. Borrmann, W. Schnelle, Y. Sun, C. Felser, and S. Medvedev, Pressure-induced superconductivity and modification of Fermi surface in type-II Weyl semimetal NbIrTe<sub>4</sub>, *npj Quantum Mater.* **6**, 55 (2021).